Design of a rapid, multiplex, one-pot miRNA assay optimized by label-free analysis

G. Zanchetta[a], T. Carzaniga[a], L. Vanjur[a], L. Casiraghi[a], G. Tagliabue[b], C. Morasso[c], T. Bellini[a], & M. Buscaglia[a,*]

[a] *Dipartimento di Biotecnologie Mediche e Medicina Traslazionale, Università degli Studi di Milano, Segrate, Italy.* [b] *Proxentia S.r.l., viale Ortles 22/4, Milano, Italy.* [c] *Nanomedicine and Molecular Imaging Laboratory, Istituti Clinici Scientifci Maugeri IRCCS, Pavia, Italy.*

**Corresponding Author. Via F.lli Cervi 93, Segrate (Milano), 20090, Italy.*
E-mail address: marco.buscaglia@unimi.it

Abstract

MicroRNAs are widely studied as circulating biomarkers for early stage diagnosis of several diseases. Detection and quantification of miRNAs is currently performed through complex and time consuming procedures. Herein we demonstrate a rapid, multiplex, one-pot detection method based on two-step amplification of the signal measured by Reflective Phantom Interface (RPI) label-free optical biosensor. We achieved sub-pM quantification of different miRNAs in about 1.5 hours, through specific capture with surface DNA probes combined to a 35-fold mass amplification by an antibody targeting DNA-RNA hybrids and polyclonal secondary antibody, all performed without washing steps. The assay is the result of a modelling and optimization of the multi-step process that has been made possible by the RPI characterization of each individual interaction involved.

Keywords: label-free biosensor; reflective phantom interface; nucleic acids; antibody; microRNA; DNA microarray; rapid detection; wash-free assay.

1. Introduction

MicroRNAs (miRNAs) are small noncoding RNAs single strands of about 22 nucleotides that function as post-transcriptional gene regulators by partially or fully pairing to mRNA targets and thus inhibiting their translation or triggering their degradation (Dong et al., 2013). It is estimated that around 2000 different miRNAs are present in humans (Alles et al., 2019), inside cells or circulating in body fluids, like blood, saliva, tears and urine. Extra-cellular miRNAs can have multiple sources, including leakage from cells, due to inflammation or apoptosis, or active release in exosomes and in protein-miRNA complexes, which also contribute to their stability against degradation (Ramshani et al., 2019)(Weber et al., 2010).

Because of their role as fine-tuners of many physiological processes, dysregulation of miRNAs has been associated to several human diseases, and their detection and quantification are being proposed for diagnostic, prognostic and therapeutic purposes (Egatz-

Gomez et al., 2016). However, the distribution of miRNAs varies significantly across the body fluids and the measurement of their low concentrations, estimated in plasma or serum between 0.1 fM and some pM (i.e. tens to millions of copies per microliter) (Cheng et al., 2010) (Kim et al., 2012) (Campomenosi et al., 2016), presents several challenges. Among these, limited sample volumes, possible interference of anti-coagulants, lack of standardized protocols for RNA extraction and purification, the need for stable small RNA species to be used as endogenous controls, all have an impact on miRNA profiling (Moldovan et al., 2014).

Currently, the main analytical methods for miRNA detection are northern blotting, real time-PCR, micro-arrays and deep sequencing. Each of them has advantages and corresponding limitations, in terms of cost, precision, accuracy, and required sample quantity. For example, PCR displays excellent sensitivity and is capable of absolute quantification, which makes it the gold standard for miRNA analysis; however, it can analyse only a small number of miRNAs in parallel. On the contrary, micro-arrays offer high throughput but have lower sensitivity and dynamic range. All these methods require a suitably furnished laboratory and numerous steps, which lead to high costs and time-to-results from several hours to days (Johnson and Mutharasan, 2014). For these reasons, the application of these methods to clinical practice and point-of-care purposes remains limited and the development of simple, low-cost and rapid assays requires alternative strategies.

Biosensor-based methods combine selective biomolecular probes for target recognition, typically represented by complementary nucleic acids strands in the case of miRNAs, and a signal transducer, often electrochemical or optical, amenable to portable devices (Johnson and Mutharasan, 2014). Biosensors represent an ideal approach for rapid, multiplexed and low-cost quantification. In the case of label-free biosensors, in which the signal is directly provided by the binding of the target molecule with the surface probe, the measurement procedure can be also very simple (Zanchetta et al., 2017). However, signal amplification is often required to achieve sufficient sensitivity to quantify target molecules in the pM range. In contrast, the direct measurement of the binding curves makes the label-free methods excellent tools for quantitative characterization of kinetics and strength of bimolecular interactions. In previous works, we have shown the use of Reflective Phantom Interface (RPI), an optical label-free biosensor based on the measurement of the intensity of light reflected by a surface with very low reflectivity, for studying a variety of interactions, including antigen-antibody (Tagliabue et al., 2017), protein-glycan (Zilio et al., 2015), and DNA-DNA (Vanjur et al., 2020). The direct, unamplified RPI signal was exploited to quantify hormones (Salina et al., 2015), biomarkers for viral infections in humans (Giavazzi et al., 2013) and plants (Salina et al., 2016), single base mismatches in DNA strand (Nava et al., 2016), and pollutants in environmental water (Lanfranco et al., 2016)(Lanfranco et al., 2018)(Lanfranco et al., 2020). Among other label-free biosensors, RPI provides the advantage of combining large sensitivity for parallel detection with low-cost disposable cartridges and compact instrumentation (Giavazzi et al., 2014).

Here we report the development of a one-pot, label-free assay based on RPI for the multiplex detection of miRNAs down to sub-pM concentrations. The assay relies on the capture of miRNA by surface-grafted complementary DNA oligomers, followed by a two-step mass amplification carried out by specific antibodies (Ab1) binding the DNA-RNA hybrids on the surface and by secondary antibodies (Ab2) further increasing the surface mass

by decorating the first antibody. The assay thus involves three different kinds of biomolecular interactions (DNA-RNA, antibody-nucleic acids and antibody-antibody) taking place in the measurement cuvette with no washing steps. Once the assay parameters are optimized through the analytical process here presented, the assay achieves sub-picomolar quantification of multiple miRNAs through a rapid and simple procedure.

2. Materials and methods

2.1 Biomolecules and reagents

We studied the interaction between different molecular partners by a RPI label-free biosensor, as described in (Salina et al., 2015). Amine-terminated DNA probe strands complementary to five different miRNA sequences were covalently immobilized in spots with 150-200 μm diameter on the surface of RPI sensing chips, previously coated with MCP4 copolymer purchased from Lucidant Polymers (Sunnyvale, CA, USA). The nucleic acids used in this work, purchased from Integrated DNA Technologies (Leuven, Belgium), are listed in Table 1. The miRNA sequences were chosen as representative examples of circulating miRNAs with known association to disease states like various human cancers and multiple sclerosis ("miRBase," 2020)(Schwarzenbach et al., 2014)(Kim et al., 2012)(Campomenosi et al., 2016)(Ferracin et al., 2015)(Li et al., 2012). Furthermore, we selected sequences with different CG contents and without significant homology. As Ab1 antibody targeting the DNA-RNA hybrid we used the S9.6 antibody, purchased from Merck-Millipore (Burlington, MA, USA). The Ab2 antibody anti-antibody was purchased from Invitrogen (Carlsbad, CA, USA). Before the measurement, the sensor cartridges were filled with 1.3 ml of measuring buffer (10 mM Tris-HCl, pH 7.5, 50 mM NaCl, 10 mM $MgCl_2$).

Table 1. miRNA and DNA strands.

Name	miRNA code	Sequence	nt
miRNA21	hsa-miR-21-5p	UAGCUUAUCAGACUGAUGUUGA	22
miRNA223	hsa-miR-223-3p	UGUCAGUUUGUCAAAUACCCCA	22
miRNA16	hsa-miR-16-5p	UAGCAGCACGUAAAUAUUGGCG	22
miRNA125	hsa-miR-125a-5p	UCCCUGAGACCCUUUAACCUGUGA	24
miRNA210	hsa-miR-210-3p	CUGUGCGUGUGACAGCGGCUGA	22
DNA21	-	/5AmMC6/TCAACATCAGTCTGATAAGCTA	22
DNA223	-	/5AmMC6/TGGGGTATTTGACAAACTGACA	22
DNA16	-	/5AmMC6/CGCCAATATTTACGTGCTGCTA	22
DNA125	-	/5AmMC6/TCACAGGTTAAAGGGTCTCAGGGA	24
DNA210	-	/5AmMC6/TCAGCCGCTGTCACACGCACAG	22
DNActrl	-	/5AmMC6/GCCCACCTATAAGGTAAAAGTGA	23

2.2 RPI measurements and analysis

The RPI measurements were performed by using the method, the apparatus and the analysis described in (Salina et al., 2015). The sensing cartridge was kept at 23 °C by a thermalized holder during the measurement. The mixing of the sample in the cartridge was provided by continuous stirring with a magnetic bar. Sample spikes of miRNAs, primary antibody or secondary antibody were performed by adding 50 µl of measuring buffer containing different amounts of such molecules. From the analysis of the time sequences of RPI images of the spotted surface, the brightness of the spots was converted into mass surface density of molecular compounds as a function of time t, $\sigma(t)$, by a custom Matlab program (Mathworks, Natick, MA, USA). The analysis was performed on averaged binding curves $\sigma(t)$ of at least 6 spots with identical composition.

In the case of RNA-DNA and antibody-hybrid interactions, the binding curves were fitted with exponential growth functions (Giavazzi et al., 2013)(Giavazzi et al., 2014) with an equilibrium plateau given by

$$\Sigma(c) = \Sigma_\infty / \left(1 + \frac{K_d}{c}\right) \tag{1}$$

where c is the concentration of the target in solution, Σ_∞ is the saturation surface density and $K_d = k_{off}/k_{on}$ is the dissociation equilibrium constant, given by the ratio between the kinetic rates for dissociation, k_{off}, and association, k_{on}. The rate $\Gamma(c)$ of the exponential binding curves is given by

$$\Gamma(c) = k_{on}c + k_{off} \tag{2}$$

The kinetic behaviour of the interactions was characterized through the initial slope of the binding curves $\sigma'(c) = \Sigma(c)\Gamma(c)$. The kinetic rate for association is then obtained from

$$k_{on} = \frac{\sigma'(c)}{\Sigma_\infty c} \tag{3}$$

In the case of the interaction between Ab2 in solution and Ab1 on the surface, the fit of the averaged binding curves $\sigma(t)$ was performed by adding an additional, slower exponential growth component and, for the largest concentrations of Ab2, a slow linear decrease. However, the analysis of the kinetic behaviour was based on the parameters obtained from the first exponential component. The overall shape of the binding curves at different concentrations of Ab2 was also evaluated by fitting with stretched exponential growth functions (see Supporting Information).

3 Results & Discussion

3.1 Assay demonstration

We designed a miRNA assay scheme based on three stages, corresponding to the addition in the same measuring solution of miRNA sample, primary antibody Ab1 targeting the DNA/RNA hybrid and secondary antibody Ab2 targeting Ab1, respectively. The assay design is schematically shown in Figure 1a. DNA probes complementary to the target miRNA sequences were immobilized as an array of spots on the surface of a RPI biosensor, consisting

of a glass prism with an anti-reflective coating optimized for water immersion. The prism was glued inside a plastic cuvette and the contained solution was kept under continuous stirring, while the miRNA and antibodies samples were added by pipetting. The binding of biomolecules on a spot corresponded to a local increase of refractive index at the prism-water interface, hence yielding an increase of reflectivity. The surface density of biomolecules on each spot was obtained analysing the time sequence of images of reflected light intensity acquired by a CCD camera upon illuminating the prism with collimated light from a LED (Salina et al., 2015).

The miRNA strands in solution form hybrids with the complementary DNA probes on the RPI surface. The binding of Ab1 to the hybrid on the surface not only enhances the label-free signal because of the larger molecular mass, but also provides multiple binding sites for the secondary antibodies Ab2. The concentrations of Ab1, c_1, and Ab2, c_2, and the measuring times were chosen in order to realize a one-pot assay, hence avoiding time-consuming and operator-dependent washing steps: the samples and the antibodies are simply sequentially added in the same solution at defined times. Figure 1b reports the surface density of molecules measured by RPI label-free sensing during the procedure. The addition of a small amount of miRNA125, corresponding to a concentration in the measuring solution of 5 pM, yields a very low signal, lower than the Limit of Detection (LOD), on spots of complementary DNA125 probe. In contrast, upon the addition of Ab1 after a time t_0, the signal markedly increases only on the DNA125 probe spots, confirming the presence of DNA/RNA hybrids. The further addition of Ab2 after an incubation time t_1 for Ab1 provides a much larger signal due to the multiple binding of secondary antibodies on Ab1 on the surface. As shown in the figure, the measured signal remains negligible on DNA spots with non-complementary sequence and on the background regions outside the DNA spots.

The performance of detection and the optimal choice of the assay parameters depend on the strength and kinetics of the three interactions involved in the three stages. The RPI label-free detection method provides both a suitable platform to implement the final assay as well as an analytical tool to fully characterize each binding step, as described in the following.

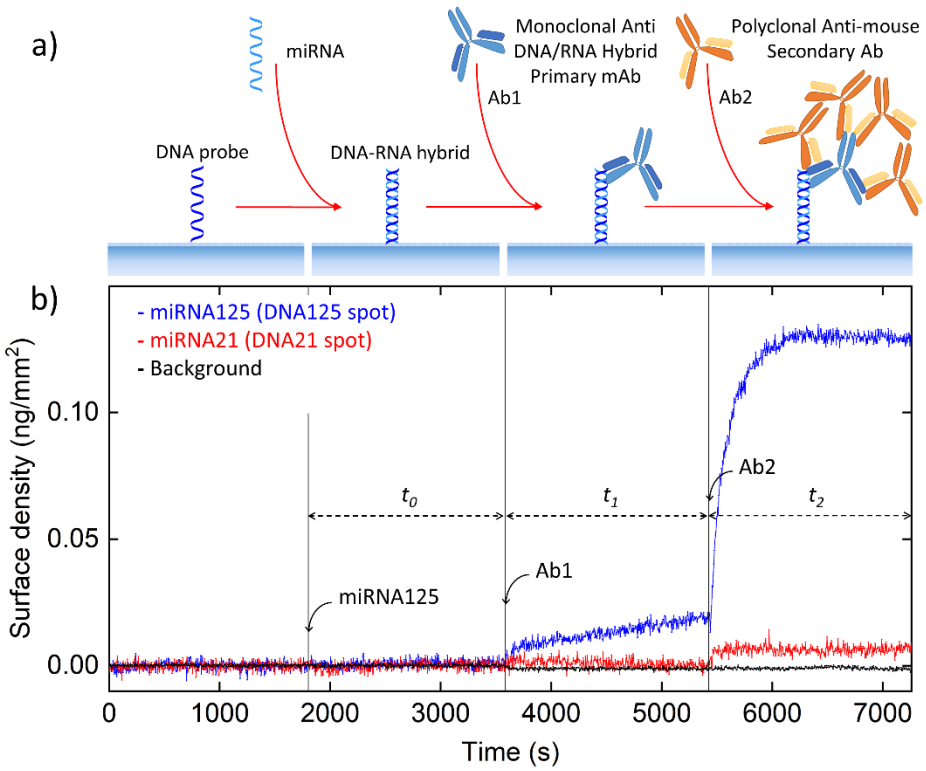

Figure 1. Assay design and demonstration. (a) A sample containing the target miRNA is injected into the RPI cartridge. The DNA probes immobilized on the surface of the RPI biosensor bind complementary miRNA in solution. After an incubation time t_0, a monoclonal antibody (Ab1) targeting the DNA/RNA hybrid is added to the solution. Then, a secondary polyclonal antibody (Ab2) that binds to Ab1 is added after a time t_1 and the measurement ends after an additional time t_2. (b) Surface density measured by RPI on spots of DNA125 (blue) and DNA21 (red) upon addition of 5 pM of miRNA125, 2.5 nM of Ab1 and 25 nM of Ab2 at the times indicated by the vertical lines. The black points represent the background signal measured outside the spots area.

3.2 Stage 1: DNA-RNA interaction on a surface

We first characterized the equilibrium and kinetics of hybridization between different miRNAs and their complementary DNA strands on the RPI surface, through sequential additions in the absence of any antibody. As shown in Figure 2a, both the amplitude and the rate of hybridization differ considerably for the miRNA sequences considered. The hybridization of miRNA21 at the concentration of 12.5 nM provides the smallest amplitude and the slowest response. In contrast, miRNA125 shows the largest and fastest signal at the same concentration. Figure 2a also shows that each family of probes only captures the miRNA with complementary strands without cross-interaction among the sequences considered in this work. This enables the parallel detection of different miRNAs with negligible interference.

In order to obtain a full characterization of DNA-RNA interaction, we analysed the binding curves measured at increasing concentration of each miRNA in solution, as reported in Figure 2b. The figure inset shows that at a concentration as low as 0.1 nM miRNA125 provided the largest signal and all measured miRNAs were well detectable except for miRNA21, whose amplitude was comparable to the background noise. The amplitudes and the initial slopes of the hybridization curves of Figure 2b, obtained by exponential fits, are

reported in Figure 2c and 2d, respectively, as a function of miRNA concentration. The fit of the amplitudes with a sigmoidal curve provided the equilibrium constant for dissociation K_d (Equation 1), whereas the initial slopes, obtained as the product between amplitude and rate of each measured hybridization curve, provided the association kinetic constant k_{on} (Equation 3). The dissociation kinetic constant was obtained as $k_{off} = K_d\ k_{on}$. The extracted values of these parameters are reported in Table 2. The values of K_d differ by less than a factor of 5 among the considered miRNA, whereas the corresponding k_{on} changes by more than a factor of 10.

The free-energy of hybridization is known to depend primarily on the sequence composition (SantaLucia, 1998). Indeed, as shown in the inset of Figure 2c, we found a monotonic dependence of the experimental K_d with the percentage of C and G in the sequence for all the miRNA except for miRNA210. Interestingly, this sequence, together with miRNA21, also showed a value of k_{on} significantly lower than the other miRNAs (Figure 2d and Table 2). To interpret this behaviour, we considered the probability of transient self-complementary interactions between target strands in solution or between the surface probe strands within the same spot for all miRNAs. These interactions are expected to compete with the binding between miRNA and DNA probe, hence reducing the effective number of available target and probe strands and the observed association rate. We indeed found that, among the considered sequences, miRNA210 and miRNA21, as well as the corresponding probes DNA210 and DNA 21, are those with the largest propensity for self-interactions, thus explaining the overestimate of K_d and the low values of k_{on} (see Supporting Information).

The difference in k_{on} among the various miRNA results in different LOD. Indeed, when aiming at detecting concentrations much smaller than K_d in a limited observation time, the resulting binding curve is only given by its initial linear growth in time, whose slope is proportional to k_{on} (Eq. 3). Therefore, given a similar surface density of DNA probes, for each miRNA the LODs will be simply proportional to the measured k_{on}, as also indicated in Figure 2d, where an equal threshold of minimum detectable initial slope (horizontal dash line) leads to distinct smallest detectable concentrations.

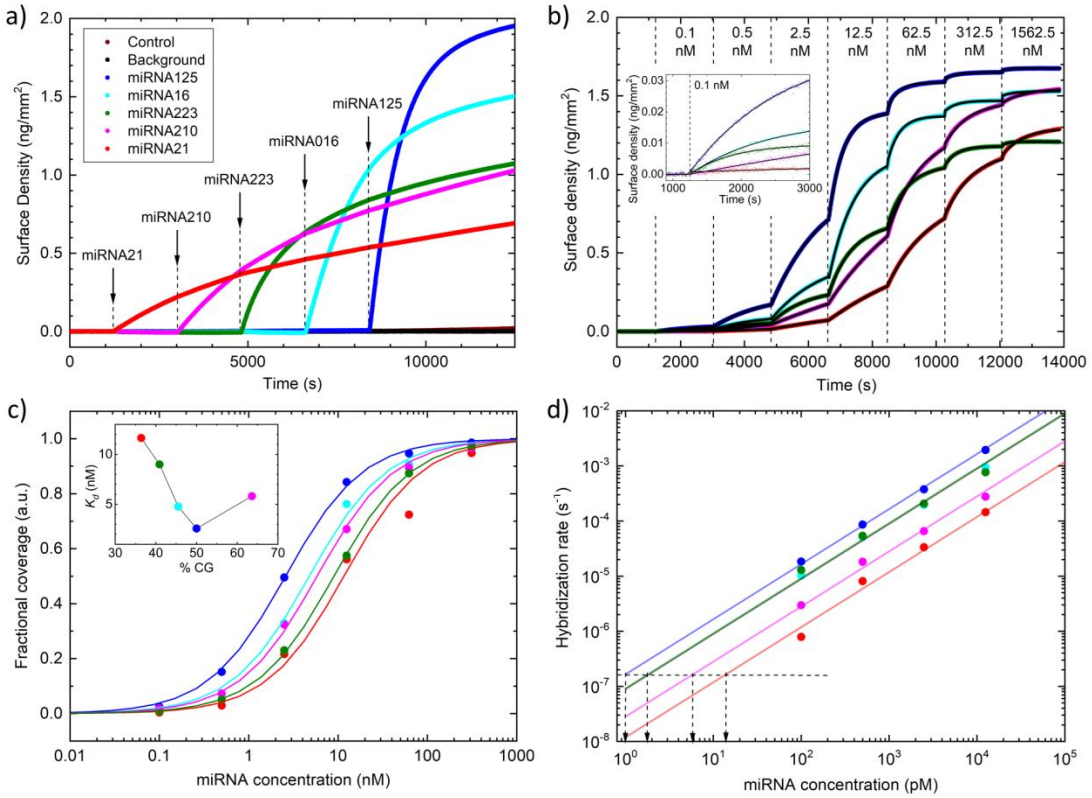

Figure 2. Characterization of miRNA-DNA hybridization. (a) Different miRNA strands were sequentially added in the same RPI cartridge at different times, as indicated by the arrows, at the concentration of 12.5 nM. The curves represent the RPI signal measured for a specific family of spots: DNA21 (red), DNA210 (magenta), DNA223 (green), DNA16 (cyan), DNA125 (blue), DNActrl (brown). Additions were ordered on purpose to favour visualization. The black line represents the background signal measured outside the spots area. (b) Surface density of miRNA on spots of complementary DNA probes measured by different RPI experiments. The concentration of miRNA is progressively increased with time, as indicated in the Figure. The black lines are fits with exponential growth curves. Inset: enlarged view of the data after the addition of 0.1 nM of miRNA. (c) Equilibrium values of surface density obtained from the exponential fits of the data reported in panel b. The lines are fit with Equation 1. Inset: K_d obtained for the different miRNAs as a function of CG content. (d) Initial hybridization rate normalized by the asymptotic surface density at saturation of probes. The continuous lines are linear fits. Dashed lines and arrows indicate the minimum concentration directly detectable for each miRNA, determined by practically measurable hybridization growth rates. The colours of panel b-d refer to spots targeting different miRNA, as reported in the legend of panel a.

Table 2. Interaction parameters measured by RPI.

Target	Surface probe	K_d (nM)	k_{off} (10^{-4} s^{-1})	k_{on} (10^4 $M^{-1}s$-1)	Measured saturation amplitude (ng/mm^2)	Max. signal amplification factor
miRNA21	DNA21	11.6	1.4	1.2	1.2	1
miRNA223	DNA223	9.0	8.3	9.2	1.2	1
miRNA16	DNA16	4.8	4.2	8.9	1.5	1
miRNA125	DNA125	2.6	4.3	16.5	1.7	1
miRNA210	DNA210	5.8	1.6	2.8	1.4	1
Ab1	DNA-RNA hybrid	0.27	0.2	7.4	12.9	21±0.7
Ab2	Ab1	18.0	10.5	15.6	85.5	168±6

3.3 Stage 2: Binding of monoclonal antibody on DNA-RNA hybrid

In the proposed assay scheme, each DNA-RNA hybrid on the surface represents a specific binding sites for Ab1 (Boguslawski et al., 1986)(Sguassero et al., 2019)(Qavi et al., 2011)(Zouari et al., 2018)(Šípová et al., 2010). We investigated a possible dependence of the Ab1-hybrid interaction on the sequence of the nucleic acid strands (König et al., 2017). An RPI sensor was prepared hybridizing the DNA probes with their corresponding miRNAs at 12.5 nM, hence at a concentration slightly larger than the K_d for all the miRNA-DNA interaction (Table 2). After an equilibration of 30 minutes, Ab1 was added to the solution at increasing concentrations. Figure 3 reports the amplitude and the initial slope (inset) obtained from exponential fits of the binding curves, both normalized by the saturation amplitude extrapolated for large concentration, which is proportional to the total number of surface binding sites. As shown in the Figure, the equilibrium dissociation constant K_d of Ab1 (i.e. the concentration corresponding to 50% fractional coverage) is very similar for all the miRNA sequences investigated. We measured a value of 0.27 nM ±0.1 nM, indicating a rather strong interaction between the antibody and the RNA-DNA hybrid. Analogously, the kinetics of the interaction is also substantially identical for the sequences considered, as reported in the inset of Figure 3. The interactions parameters extracted from the analysis are reported in Table 2. As commonly observed, the low K_d of the Ab1 binding is primarily due to the long dissociation time, as indicated by the low value of k_{off}.

The Ab1 molecular mass is about 21 times larger than that of miRNAs, therefore we assumed this as the maximum amplification factor for label-free sensing. In practice, this enhancement of the signal is achieved only at large concentrations of Ab1 and at low surface density of DNA-RNA hybrid, a condition in which the Ab1 antibodies are far apart from each other on the surface. In such condition, despite the significant amplification, the overall RPI signal is low. In contrast, at large surface density of hybrids, where the RPI signal is larger, the maximum surface density of Ab1 is limited by the antibody size. This fact can be appreciated from the data reported in Table 2, obtained for rather large hybrid surface density. The values of the asymptotic amplitudes at saturation indicate that despite the larger difference in molecular mass, the amplification factor relative to the miRNA signal obtained for Ab1 at saturation is of only 9.5±1.4, a condition which corresponds to a smaller molecular surface number density of Ab1 vs. hybrids, as a result of the steric hindrance between Ab1 molecules.

3.4 Stage 3: Signal amplification by polyclonal secondary antibody

The rather small value of K_d for Ab1-hybrid binding enables to reach a large fractional coverage of hybrid binding sites at Ab1 concentrations c_1 as small as a few nM. This offers the opportunity to exploit a further amplification step based on the addition of a larger concentration of secondary antibodies without the need of removing the Ab1 antibodies from the solution. Moreover, using a polyclonal antibody Ab2 anti-Ab1, multiple secondary antibodies can bind a single primary antibody, hence providing a further amplification factor. In order to properly design this stage of the assay, we investigated the binding of Ab2 on Ab1 previously bound to the DNA-RNA hybrid, while Ab1 is still present in solution at a concentration of 2.5 nM, corresponding to about 10 times the K_d for Ab1-hybrid binding.

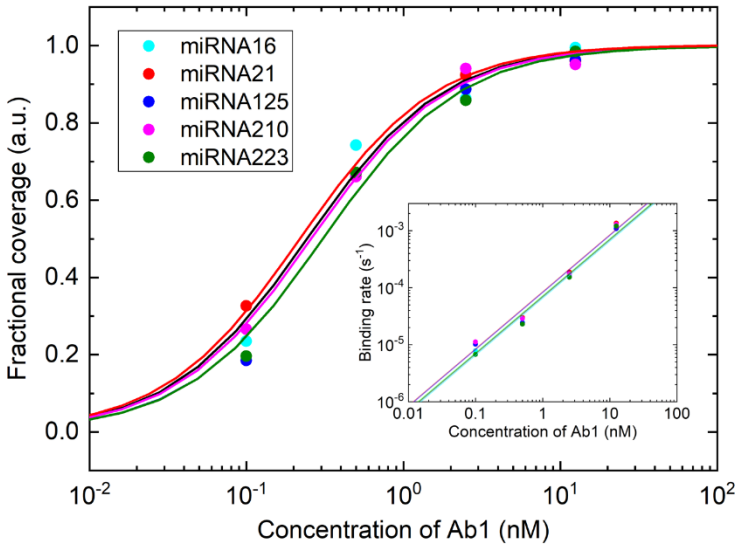

Figure 3. Characterization of Ab1 binding to miRNA-DNA hybrid. Fractional coverage of Ab1 on spots of DNA probes hybridized with complementary miRNA at 12.5 nM for 30 minutes. Symbols correspond to different DNA probe spots, targeting the miRNAs indicated in the Figure, while the curves are fits with Eq. 1. Inset: initial binding rate normalized by the asymptotic surface density at saturation. The lines are linear fits.

Figure 4a reports the binding curves measured for repeated experiments performed at different Ab2 concentrations c_2. The binding of Ab2 on Ab1 on the surface is very low for $c_2 < c_1$ and becomes larger and faster with increasing c_2. The binding curves also change shape at different c_2, from a single exponential growth at small concentrations to a more complex behaviour at larger concentrations.

Figure 4b shows an enlarged view of the data in the early stages of Figure 4a. In the first 5 minutes the binding curves are all well fitted by single exponential growth functions. At the maximum concentration of Ab2, the measured amplitude corresponds to about 4 times the signal of the underlying Ab1 layer. The amplitudes and the rates as a function of Ab2 concentration in solution are reported as open circles in Figure 4c and 4d, respectively. The observed dependence of the amplitudes can be fitted by the Hill-Langmuir equation with exponent about 1.7 (dashed line in Figure 4c, see caption). Remarkably, the same exponent is also found fitting the scaling of the initial slope of the binding curves, as shown in the inset of Figure 4d. This behaviour is due to the fact that the concentration of freely available Ab2 does not correspond to the added concentration c_2, in general, because a fraction of Ab2 antibodies bind to Ab1 still present in solution (see Supporting Information). Figures 4c and 4d report as black circles the data corrected for the concentration of available Ab2 in solution, from which the equilibrium and kinetics parameters of the first exponential component are derived (Table 2).

The full binding curves over a longer time interval are well fitted by double exponential or stretched exponential functions plus a linear decrease (see Supporting Information). The stretching exponent is reported in the inset of Figure 4c and shows that the binding curves become progressively less exponential upon increasing c_2. These fits enable to estimate the

maximum amplitude reached by the Ab2 binding curves (triangles in Figure 4c), which corresponds to a ratio Ab2:Ab1 of about 7. The measured saturation mass of Ab2 antibodies is reported in Table 2. The maximum cumulative amplification factor that one could expect simply based on the ratio between the mass of the miRNA-DNA hybrids and the maximum total mass of Ab1 and Ab2 that can accumulate on them is about 168. However, this theoretical amplification can be achieved only at large concentrations of antibodies and long incubation times.

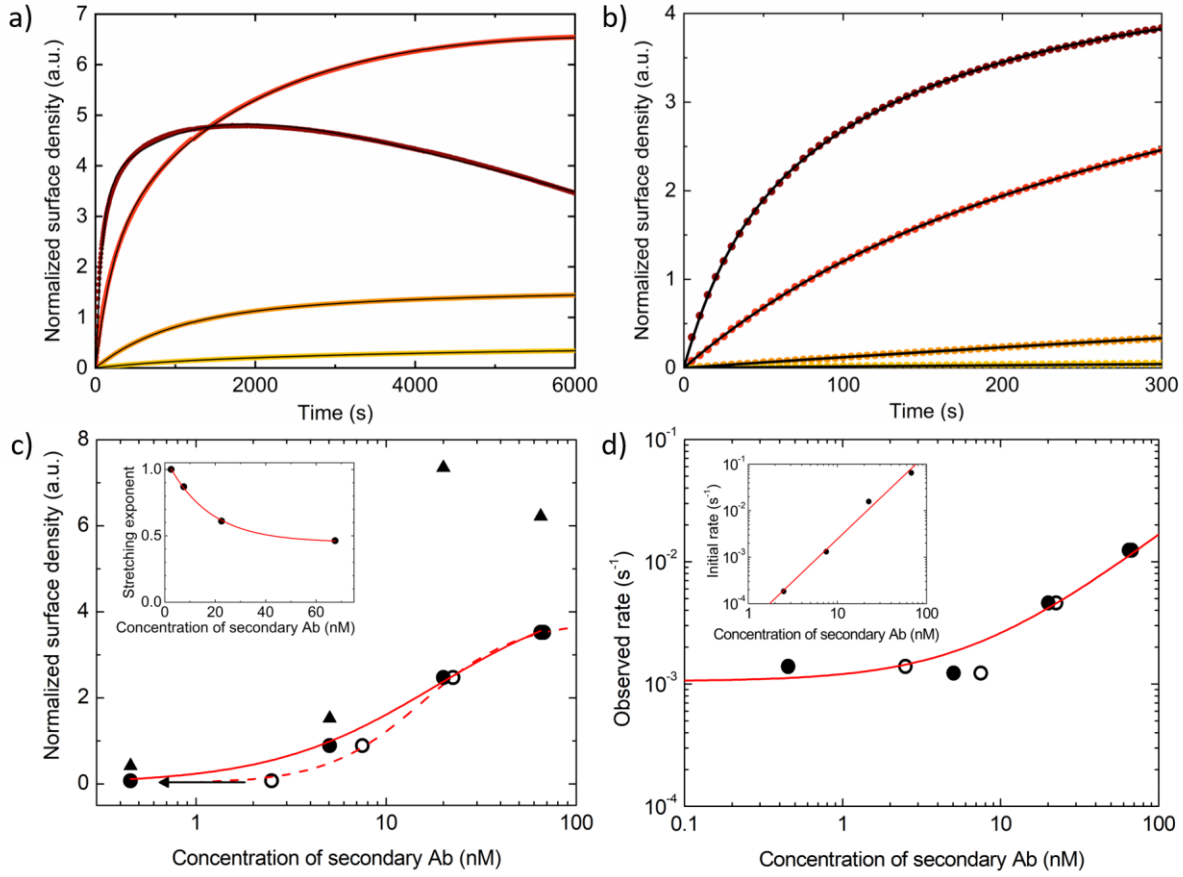

Figure 4. Characterization of Ab2 binding to Ab1. (a) Surface density of Ab2 accumulating on Ab1, normalized to the initial value given by Ab1 only, after the addition of Ab2 in solution at the concentration of 2.5 nM (yellow), 7.5 nM (orange), 22.5 nM (red) and 67.5 nM (brown) in different RPI cartridges previously incubated with 12.5 nM of miRNA125 for 30 minutes and then with 2.5 nM of Ab1 for 45 minutes. The black curves are fits with single exponential growth (yellow), double exponential growth (orange), double exponential growth and a linear decrease (red and brown). (b) Enlarged view of the data of panel a. (c) Asymptotic equilibrium values of the double exponential growth (triangles) and of the rapid relaxation contribution obtained from the fit of curves of panel a as a function of the total concentration of Ab2 in solution (open circles) and of the concentration corrected by the competitive effect with Ab1 in solution (full circles). The red lines are fits with Hill-Langmuir equation $\Sigma/\Sigma_\infty=(1+(K_d/c)^p)^{-1}$ with p = 1.73 (dashed line) and p = 1 (continuous line). Inset: exponent of stretched exponential fits of the curves of panel a. (d) Observed binding rate of the rapid relaxation contribution obtained from the fit of panel a curves as a function of the total concentration of Ab2 in solution (open circles) and of the concentration corrected by the competitive effect with Ab1 in solution (full circles). The red curve is a linear fit of full circles data points. Inset: initial slope of the curves of panel a (dots) and power law fit with exponent 1.72.

3.5 Modelling and validation of assay performance

The label-free characterization of the three individual interactions involved in the assay enables a quantitative modelling of its output signal. From the kinetic constants and the amplification factors reported in Table 2, we simulated the amount of surface bound miRNA, Ab1 and Ab2 at various concentrations and incubation times as obtained by a system of consecutive kinetic equations. The model is described in the Supporting Information. The behaviour expected from the model is shown in Figure 5a, which reports the amplification factor, defined as the ratio between the signal of the complete assay, containing miRNA, Ab1 and Ab2 and that of miRNA only, computed at different incubation times t_0, t_1 and t_2, with the constraint of a total incubation time $t_0 + t_1 + t_2 = 1.5$ hours. As shown in the figure, an amplification factor larger than 30 is obtained with rather long incubation times for Ab1 and for t_2 between 5 and 20 minutes. In contrast, the incubation time for the miRNAs alone should be kept very short, within a few minutes. According to this scheme, Figure 5b shows the amplification factor as a function of Ab1 concentration for different choices of t_2 (and t_1), while keeping $t_0 = 1$ min. The optimal concentration c_1 is about 4.5 nM, which leads to an amplification factor close to 35.

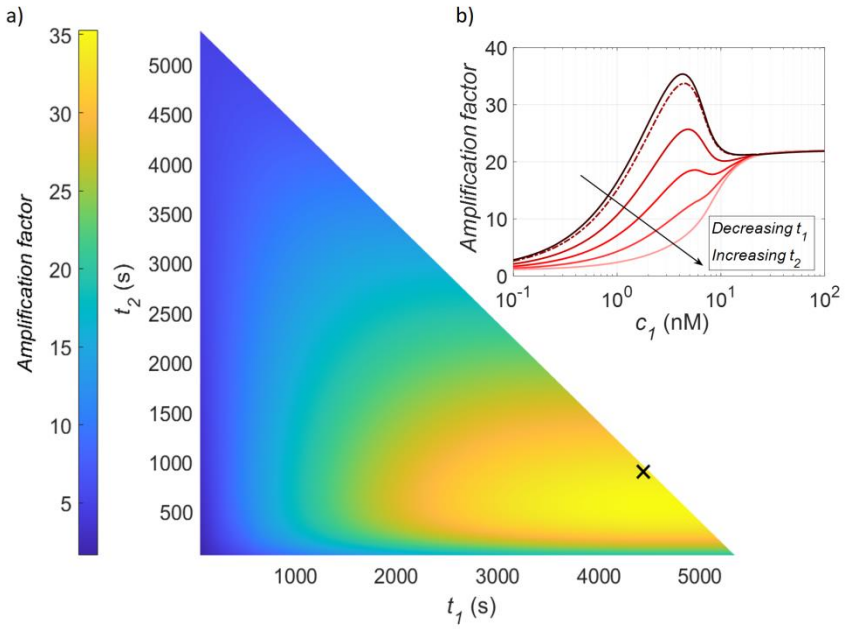

Figure 5. Simulated amplification factor as a function of incubation parameters. (a) Amplification factor for different incubation times calculated with the constraint $t_0 + t_1 + t_2 = 1.5$ hours and for $c_1 = 4.5$ nM and $c_2 = 25$ nM. (b) Amplification factor as a function of c_1 computed for different t_1 and t_2 while keeping $c_2 = 25$ nM, $t_0 = 1$ min and the total measurement time to 1.5 hours. The arrow indicates how the curves change decreasing t_1 (increasing t_2). The plotted curves correspond to values of t_1 of 79 min, 74 min, 59 min, 44.5 min, 30 min and 15 min. The assay parameters used for the measurements reported in Figure 6 are indicated by an 'X' in panel a, and as a dashed line in panel b. Full details on the simulation are reported in Supplementary Information.

On the basis of this analysis, we experimentally studied the response of the assay close to the simulated optimal conditions (t_0 = 1 min, t_1 = 74 min, t_2 = 15 min) and for different concentrations of miRNAs, down to 0.5 pM. We spiked mixtures of the five miRNAs prepared with relative concentrations inversely proportional to the values of their k_{on} for

binding with the surface DNA probes. Indeed, at concentrations much lower than the dissociation constant, the binding curves of miRNA-DNA interactions, although remaining below the instrumental sensitivity, are expected to increase linearly with time, with a slope proportional to k_{on} (Equation 3). The results are reported in Figure 6, which demonstrates a linear response of the final Ab2 signal across almost two orders of magnitude of miRNA concentration, which enables to capture the 2- to 10-fold dysregulation reported in literature for several disease states (Li et al., 2012)(Motamedi et al., 2019). As expected, we obtained the maximum sensitivity for miRNA125, followed by miRNA16 and miRNA223. In order to estimate the LOD, we measured the background signal on control spots (see Supporting Information) and computed the miRNA concentrations corresponding to 3σ above such background (grey area in Figure 6). The LODs of miRNA125, miRNA16 and miRNA223 are 0.3 pM, 0.7 pM and 0.75 pM, respectively. In contrast, miRNA21 and miRNA210 provide LODs of 4.1 pM and 6.7 pM, respectively.

The results in Figure 6 demonstrate that sub-picomolar detection is achieved in a one-pot assay without enzyme- or nanoparticle-based amplification through a fine tuning of the assay parameters. Methods for miRNA extraction from plasma or other biological fluids typically result in rather clean samples suspended in buffer, with 100-fold enrichment of RNA content (Wright et al., 2020); therefore, we anticipate similar performances of our assay when used with these samples. Given the literature values for freely circulating concentrations of the miRNAs studied here and considering such enrichment factor, our LODs are either well within physiological estimates of 10-100 fM for miRNA16 (Schwarzenbach et al., 2014), or still about a factor of ten larger than 0.1 fM for miRNA125 and 1 fM for miRNA21 (Campomenosi et al., 2016).

According to literature, the sensitivity for miRNA quantification varies significantly depending on the detection approach (D'Agata and Spoto, 2019). LODs in the sub-picomolar range have been so far reported only for methods exploiting enzymatic enhancement or making use of gold nanoparticles to enhance the signal of label-free biosensors (Sguassero et al., 2019). In contrast, non-enzymatic amplification methods achieved only by antibodies and proteins commonly display larger detection limits (Šípová et al., 2010)(Ding et al., 2015). The better sensitivity of the method here presented is for the most part the outcome of having accessed all stages of the interactions and having undergone a quantitative optimization.

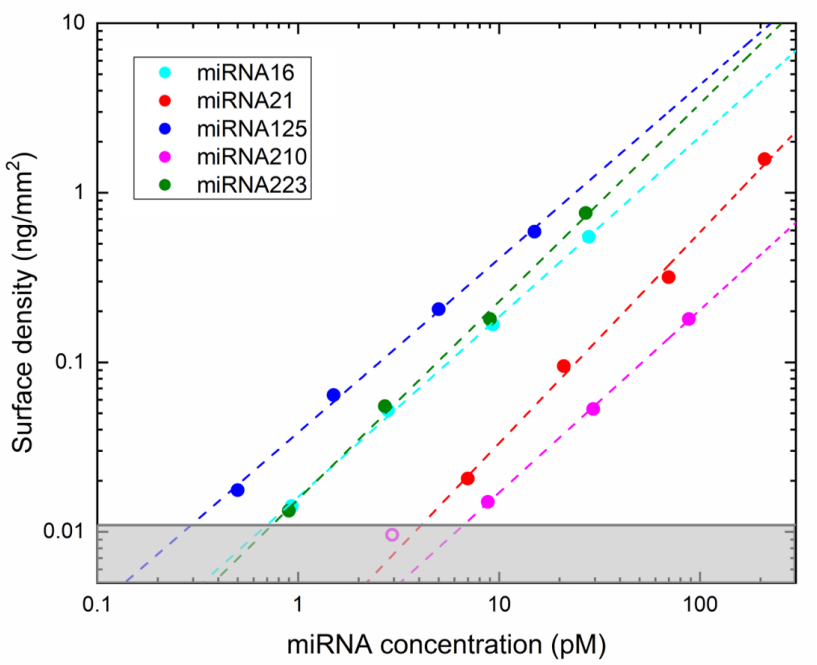

Figure 6. Assay response measured by experiments. Maximum signal measured after the addition of Ab2 for different concentrations of the miRNAs. The assay parameters are t_0 = 1 min, t_1 = 74 min, t_2 = 15 min, c_1 = 4.5 nM and c_2 = 25 nM. Dashed lines are fits with power law functions. The average exponent obtained from the fitting curve was 1.1 ± 0.09. The open magenta point was excluded from the fit. The shade grey area represents the signal values within 3σ from the background level measured on control spots.

4 Conclusions

We demonstrated sub-pM detection and linear response with a good dynamic range of different miRNAs by RPI optical label-free biosensor, using disposable, single-use cartridges. We propose a one-pot detection scheme that avoids washing steps and calibration and is based on three sequential interactions, finely tuned and optimized thanks to a preliminary characterization of each interaction. The combined effect of mass and concentration increase yields to a maximum theoretical amplification factor of the RPI signal of more than one hundred relative to the direct label-free measurement of miRNA alone. However, in order to limit the overall measuring time, we chose to keep the total incubation time to 1.5 h, hence obtaining a theoretical amplification factor of 35. Moreover, the proposed method only requires the addition of antibody reagents at established times after the addition of the miRNA sample. Therefore, the measuring procedure is simpler and more rapid than the standard methods currently in use, which typically require a suitably furnished laboratory and specialized personnel.

The analysis of the single interactions involved in the assay and their theoretical modelling provided important insights on the different factors affecting the current sensitivity of the approach. The overall performance is found to depend on the specific miRNA sequence in two ways: (i) the strength of the interaction with the surface DNA probe scales with the CG content of the sequence; (ii) the strength of partial self-hybridization of the DNA probes and miRNAs due to partial self-complementarity of the sequence has a direct effect on miRNA-

DNA binding, hence limiting the overall sensitivity of the assay for a given measuring time. Moreover, the simulation of the amplification factor obtained in various conditions provides a tool to optimize the assay by balancing the total measuring time and the sensitivity of detection at low concentration of miRNAs. Overall, these results are expected to foster and guide the design and development of other miRNA arrays, possibly including those based on more standard detection methods, such as fluorescence or chemiluminescence. Further studies will be needed to effectively combine the proposed assay scheme with a suitable extraction protocol to obtain miRNA samples with adequate concentration and purity from biological fluids.

Acknowledgements

We thank ProXentia Srl (Milano, Italy) for providing the RPI sensing cartridges. We also thank Massimo Locati for useful discussions. This work has received funding from Regione Lombardia and FESR, through the NeOn project (ID 239047).

References

Alles, J., Fehlmann, T., Fischer, U., Backes, C., Galata, V., Minet, M., Hart, M., Abu-Halima, M., Grässer, F.A., Lenhof, H.-P., Keller, A., Meese, E., 2019. An estimate of the total number of true human miRNAs. Nucleic Acids Res. 47, 3353–3364. https://doi.org/10.1093/nar/gkz097

Boguslawski, S.J., Smith, D.E., Michalak, M.A., Mickelson, K.E., Yehle, C.O., Patterson, W.L., Carrico, R.J., 1986. Characterization of monoclonal antibody to DNA · RNA and its application to immunodetection of hybrids. J. Immunol. Methods 89, 123–130. https://doi.org/10.1016/0022-1759(86)90040-2

Campomenosi, P., Gini, E., Noonan, D.M., Poli, A., D'Antona, P., Rotolo, N., Dominioni, L., Imperatori, A., 2016. A comparison between quantitative PCR and droplet digital PCR technologies for circulating microRNA quantification in human lung cancer. BMC Biotechnol. 16, 60. https://doi.org/10.1186/s12896-016-0292-7

Cheng, Y., Tan, N., Yang, J., Liu, X., Cao, X., He, P., Dong, X., Qin, S., Zhang, C., 2010. A translational study of circulating cell-free microRNA-1 in acute myocardial infarction. Clin. Sci. 119, 87–95. https://doi.org/10.1042/CS20090645

D'Agata, R., Spoto, G., 2019. Advanced methods for microRNA biosensing: a problem-solving perspective. Anal. Bioanal. Chem. 411, 4425–4444. https://doi.org/10.1007/s00216-019-01621-8

Ding, X., Yan, Y., Li, S., Zhang, Y., Cheng, W., Cheng, Q., Ding, S., 2015. Surface plasmon resonance biosensor for highly sensitive detection of microRNA based on DNA super-sandwich assemblies and streptavidin signal amplification. Anal. Chim. Acta 874, 59–65. https://doi.org/10.1016/j.aca.2015.03.021

Dong, H., Lei, J., Ding, L., Wen, Y., Ju, H., Zhang, X., 2013. MicroRNA: Function, Detection, and Bioanalysis. Chem. Rev. 113, 6207–6233. https://doi.org/10.1021/cr300362f

Egatz-Gomez, A., Wang, C., Klacsmann, F., Pan, Z., Marczak, S., Wang, Y., Sun, G., Senapati, S., Chang, H.-C., 2016. Future microfluidic and nanofluidic modular platforms for nucleic acid liquid biopsy in precision medicine. Biomicrofluidics 10, 032902. https://doi.org/10.1063/1.4948525

Ferracin, M., Lupini, L., Salamon, I., Saccenti, E., Zanzi, M.V., Rocchi, A., Da Ros, L., Zagatti, B., Musa, G., Bassi, C., Mangolini, A., Cavallesco, G., Frassoldati, A., Volpato, S., Carcoforo, P., Hollingsworth, A.B., Negrini, M., 2015. Absolute quantification of cell-free microRNAs in cancer patients. Oncotarget 6, 14545-14555. https://doi.org/10.18632/oncotarget.3859

Giavazzi, F., Salina, M., Ceccarello, E., Ilacqua, A., Damin, F., Sola, L., Chiari, M., Chini, B., Cerbino, R., Bellini, T., Buscaglia, M., 2014. A fast and simple label-free immunoassay based on a smartphone. Biosens. Bioelectron. 58, 395–402. https://doi.org/10.1016/j.bios.2014.02.077

Giavazzi, F., Salina, M., Cerbino, R., Bassi, M., Prosperi, D., Ceccarello, E., Damin, F., Sola, L., Rusnati, M., Chiari, M., Chini, B., Bellini, T., Buscaglia, M., 2013. Multispot, label-free biodetection at a phantom plastic–water interface. Proc. Natl. Acad. Sci. 110, 9350–9355. https://doi.org/10.1073/pnas.1214589110

Johnson, B.N., Mutharasan, R., 2014. Biosensor-based microRNA detection: techniques, design, performance, and challenges. Analyst 139, 1576-1588. https://doi.org/10.1039/c3an01677c

Kim, D.-J., Linnstaedt, S., Palma, J., Park, J.C., Ntrivalas, E., Kwak-Kim, J.Y.H., Gilman-Sachs, A., Beaman, K., Hastings, M.L., Martin, J.N., Duelli, D.M., 2012. Plasma Components Affect Accuracy of Circulating Cancer-Related MicroRNA Quantitation. J. Mol. Diagnostics 14, 71–80. https://doi.org/10.1016/j.jmoldx.2011.09.002

König, F., Schubert, T., Längst, G., 2017. The monoclonal S9.6 antibody exhibits highly variable binding affinities towards different R-loop sequences. PLoS One 12, e0178875. https://doi.org/10.1371/journal.pone.0178875

Lanfranco, R., Giavazzi, F., Bellini, T., Di Nicolò, E., Buscaglia, M., 2020. Fabrication and Optical Modeling of Micro-Porous Membranes Index-Matched with Water for On-Line Sensing

Applications. Macromol. Mater. Eng. 305, 1900701. https://doi.org/10.1002/mame.201900701

Lanfranco, R., Giavazzi, F., Salina, M., Tagliabue, G., Di Nicolò, E., Bellini, T., Buscaglia, M., 2016. Selective Adsorption on Fluorinated Plastic Enables the Optical Detection of Molecular Pollutants in Water. Phys. Rev. Appl. 5, 054012. https://doi.org/10.1103/PhysRevApplied.5.054012

Lanfranco, R., Saez, J., Di Nicolò, E., Benito-Lopez, F., Buscaglia, M., 2018. Phantom membrane microfluidic cross-flow filtration device for the direct optical detection of water pollutants. Sensors Actuators B Chem. 257, 924–930. https://doi.org/10.1016/j.snb.2017.11.024

Li, B., Zhao, Y., Guo, G., Li, W., Zhu, E., Luo, X., Mao, X., Zou, Q., Yu, P., Zuo, Q., Li, N., Tang, B., Liu, K., Xiao, B., 2012. Plasma microRNAs, miR-223, miR-21 and miR-218, as Novel Potential Biomarkers for Gastric Cancer Detection. PLoS One 7, e41629. https://doi.org/10.1371/journal.pone.0041629

miRBase [WWW Document], 2020. URL www.mirbase.org

Moldovan, L., Batte, K.E., Trgovcich, J., Wisler, J., Marsh, C.B., Piper, M., 2014. Methodological challenges in utilizing miRNAs as circulating biomarkers. J. Cell. Mol. Med. 18, 371–390. https://doi.org/10.1111/jcmm.12236

Motamedi, M., Hashemzadeh Chaleshtori, M., Ghasemi, S., Mokarian, F., 2019. Plasma Level Of miR-21 And miR-451 In Primary And Recurrent Breast Cancer Patients. Breast Cancer Targets Ther. 11, 293–301. https://doi.org/10.2147/BCTT.S224333

Nava, G., Ceccarello, E., Giavazzi, F., Salina, M., Damin, F., Chiari, M., Buscaglia, M., Bellini, T., Zanchetta, G., 2016. Label-free detection of DNA single-base mismatches using a simple reflectance-based optical technique. Phys. Chem. Chem. Phys. 18, 13395–13402. https://doi.org/10.1039/C5CP08017G

Qavi, A.J., Kindt, J.T., Gleeson, M.A., Bailey, R.C., 2011. Anti-DNA:RNA Antibodies and Silicon Photonic Microring Resonators: Increased Sensitivity for Multiplexed microRNA Detection. Anal. Chem. 83, 5949–5956. https://doi.org/10.1021/ac201340s

Ramshani, Z., Zhang, C., Richards, K., Chen, L., Xu, G., Stiles, B.L., Hill, R., Senapati, S., Go, D.B., Chang, H.-C., 2019. Extracellular vesicle microRNA quantification from plasma using an integrated microfluidic device. Commun. Biol. 2, 189. https://doi.org/10.1038/s42003-019-0435-1

Salina, M., Giavazzi, F., Ceccarello, E., Damin, F., Chiari, M., Ciuffo, M., Accotto, G.P., Buscaglia, M., 2016. Multi-spot, label-free detection of viral infection in complex media by a non-reflecting surface. Sensors Actuators B Chem. 223, 957–962. https://doi.org/10.1016/j.snb.2015.09.122

Salina, M., Giavazzi, F., Lanfranco, R., Ceccarello, E., Sola, L., Chiari, M., Chini, B., Cerbino, R., Bellini, T., Buscaglia, M., 2015. Multi-spot, label-free immunoassay on reflectionless glass. Biosens. Bioelectron. 74, 539–545. https://doi.org/10.1016/j.bios.2015.06.064

SantaLucia, J., 1998. A unified view of polymer, dumbbell, and oligonucleotide DNA nearest-neighbor thermodynamics. Proc. Natl. Acad. Sci. 95, 1460–1465. https://doi.org/10.1073/pnas.95.4.1460

Schwarzenbach, H., Nishida, N., Calin, G.A., Pantel, K., 2014. Clinical relevance of circulating cell-free microRNAs in cancer. Nat. Rev. Clin. Oncol. 11, 145–156. https://doi.org/10.1038/nrclinonc.2014.5

Sguassero, A., Artiga, Á., Morasso, C., Jimenez, R.R., Rapún, R.M., Mancuso, R., Agostini, S., Hernis, A., Abols, A., Linē, A., Gualerzi, A., Picciolini, S., Bedoni, M., Rovaris, M., Gramatica, F., de la Fuente, J.M., Vanna, R., 2019. A simple and universal enzyme-free approach for the detection of multiple microRNAs using a single nanostructured enhancer of surface plasmon resonance imaging. Anal. Bioanal. Chem. 411, 1873–1885. https://doi.org/10.1007/s00216-018-1331-0

Šípová, H., Zhang, S., Dudley, A.M., Galas, D., Wang, K., Homola, J., 2010. Surface Plasmon

Resonance Biosensor for Rapid Label-Free Detection of Microribonucleic Acid at Subfemtomole Level. Anal. Chem. 82, 10110–10115. https://doi.org/10.1021/ac102131s

Tagliabue, G., Faoro, V., Rizzo, S., Sblattero, D., Saccani, A., Riccio, G., Bellini, T., Salina, M., Buscaglia, M., Marcello, A., 2017. A label-free immunoassay for Flavivirus detection by the Reflective Phantom Interface technology. Biochem. Biophys. Res. Commun. 492, 558–564. https://doi.org/10.1016/j.bbrc.2017.05.025

Vanjur, L., Carzaniga, T., Casiraghi, L., Chiari, M., Zanchetta, G., Buscaglia, M., 2020. Non-Langmuir kinetics of DNA surface hybridization. Biophysical Juornal 119 (5), 989-1001. https://doi.org/10.1016/j.bpj.2020.07.016

Weber, J.A., Baxter, D.H., Zhang, S., Huang, D.Y., How Huang, K., Jen Lee, M., Galas, D.J., Wang, K., 2010. The MicroRNA Spectrum in 12 Body Fluids. Clin. Chem. 56, 1733–1741. https://doi.org/10.1373/clinchem.2010.147405

Wright, K., de Silva, K., Purdie, A.C., Plain, K.M., 2020. Comparison of methods for miRNA isolation and quantification from ovine plasma. Sci. Rep. 10, 825. https://doi.org/10.1038/s41598-020-57659-7

Zanchetta, G., Lanfranco, R., Giavazzi, F., Bellini, T., Buscaglia, M., 2017. Emerging applications of label-free optical biosensors. Nanophotonics 6 (4), 627-645. https://doi.org/10.1515/nanoph-2016-0158

Zilio, C., Bernardi, A., Palmioli, A., Salina, M., Tagliabue, G., Buscaglia, M., Consonni, R., Chiari, M., 2015. New “clickable” polymeric coating for glycan microarrays. Sensors Actuators, B Chem. 215, 412-420. https://doi.org/10.1016/j.snb.2015.03.079

Zouari, M., Campuzano, S., Pingarrón, J.M., Raouafi, N., 2018. Amperometric Biosensing of miRNA-21 in Serum and Cancer Cells at Nanostructured Platforms Using Anti-DNA–RNA Hybrid Antibodies. ACS Omega 3, 8923–8931. https://doi.org/10.1021/acsomega.8b00986

Supporting Information

Design of a rapid, multiplex, one-pot miRNA assay optimized by label-free analysis

G. Zanchetta[a], T. Carzaniga[a], L. Vanjur[a], L. Casiraghi[a], G. Tagliabue[b], C. Morasso[c], T. Bellini[a], & M. Buscaglia[a]

[a] *Dipartimento di Biotecnologie Mediche e Medicina Traslazionale, Università degli Studi di Milano, Segrate, Italy.* [b] *Proxentia S.r.l., viale Ortles 22/4, Milano, Italy.* [c] *Nanomedicine and Molecular Imaging Laboratory, Istituti Clinici Scientifci Maugeri IRCCS, Pavia, Italy.*

S1 Effect of partial self-complementarity on DNA-RNA hybridization

As mentioned in the main text, if the sequence of a specific miRNA (and of the corresponding DNA probe) is partially self-complementary, as e.g. in the case of miRNA210, the estimate of K_d can be affected for two main reasons, related to DNA surface probes and RNA strands in solution. First, DNA strands within the same spot can transiently hybridize, thus effectively reducing the number of available probes and the measured association rate with miRNA targets, and therefore overestimating K_d (Nava et al., 2016). To quantify this effect, through nearest-neighbour parameters (SantaLucia, 1998)(Weber, 2015) we estimated for each DNA probe the free energy of self-hybridization and the fraction of self-paired strands in the experimental conditions (taking into account that the local, effective concentration of probes is large due to their surface confinement, up to the mM range), in competition with the full pairing with the RNA target. Adopting a simple kinetic model used in (Nava et al., 2016) to account for weak, nonspecific surface binding, we found that K_d is significantly affected, even by an order of magnitude, mostly for miRNA210 and miRNA21 because of their sequence pattern, while the degree of self-complementarity and corresponding weakening are less important for the other miRNAs. Given the uncertainty in the estimate of effective concentration of DNA probes, however, we reported uncorrected K_d values in Figure 2c inset.

Furthermore, if a fraction of miRNA strands in solution can self-pair, their binding with DNA probes is weakened, which effectively reduces the solution concentration of miRNA, again leading to an overestimate of K_d. We estimated with NUPACK (Zadeh et al., 2011) the fraction of self-paired strands for each miRNA strand in solution at the various experimental concentrations, and estimated K_d with corrected concentrations. We found for miRNA210, the RNA strand with the largest degree of self-complementarity, a K_d reduction of less than 10%.

S2 Analysis of secondary antibody binding curves

The interactions between miRNAs in solution and surface immobilized DNA strands, as well as that between antibody Ab1 in solution and the DNA-RNA hybrids on the surface, were analysed assuming an ideal Langmuir binding model. Accordingly, each binding curve representing the molecular surface density σ as a function of the time t after a stepwise increase of target concentration c was fitted with an exponential growth function given by (Giavazzi et al., 2013)(Giavazzi et al., 2014)

$$\sigma(t) = \Sigma(c)(1 - e^{-\Gamma(c)t}) \tag{S1}$$

where the asymptotic amplitude Σ depends on equilibrium constant K_d and the rate Γ depends on the kinetic rate constants for association k_{on} and dissociation k_{off}, as described in the main text (Material and Methods). In contrast, in the case of the interaction between Ab2 in solution and Ab1 on the surface, the observed binding curves clearly deviated from a single exponential shape, at least for large enough concentration of Ab2. Moreover, at the largest concentrations, we observed non-monotonic binding curves showing a slow decrease at long times. Therefore, in this case the fit of the binding curves $\sigma(t)$ was performed by using more complex functions. We fitted the Ab2 binding curves with two different functions: (i) a sum of two exponential growth functions and a linear decrease and (ii) a sum of a stretched exponential growth function and a linear decrease. The fitting function (i) is given by

$$\sigma(t) = \Sigma(1 - e^{-\Gamma t}) + \Sigma_2(1 - e^{-\Gamma_2 t}) - St \tag{S2}$$

where the amplitude Σ_2 of the second exponential term and the linear coefficient S are set to zero for the smallest concentrations of Ab2, at which the shape of the binding curve is indistinguishable from a single exponential growth. The analysis of the kinetic behaviour was solely based on the parameters obtained from the first exponential component. The fitting function (ii) was given by

$$\sigma(t) = A\left(1 - e^{-(kt)^{\beta}}\right) - St \tag{S3}$$

where the linear coefficient S was set to zero at the smallest concentrations and left free to vary only at the largest concentrations, at which the binding curves clearly showed a non-monotonic behaviour with time. The stretching exponent β was found to vary from 1 to about 0.5 increasing the concentration of Ab2 in solution (inset of Figure 4c in the main text).

S3 Effect of Ab1-Ab2 interaction in solution

In the case of DNA-RNA and Ab1-hybrid binding, the interaction can take place only on the surface because there are no probe DNA or hybrids in solution. In contrast, the binding of Ab2 with Ab1 can take place either in solution or on the surface. Therefore, the modelling of the behaviour of the molecular interactions becomes more complex after the addition of Ab2, because both the concentrations of free Ab2 and Ab1 are affected by their reciprocal interaction in solution. In general, the addition of Ab2 at a concentration c_2 in a sample already containing Ab1 at a concentration c_1, yields to a lower amount of available Ab2 and

Ab1 for the surface binding. Assuming that the formation of Ab1-Ab2 pairs in solution happens much faster than that on the surface, this interaction can be treated as at equilibrium for the experimental time resolution of the surface assay. We considered a simple bimolecular interaction, in which each Ab1 molecule provides n_1 binding sites for Ab2 and each Ab2 molecule provides n_2 binding sites for Ab1. The value of n_2 is 2, as for any IgG antibody binding through its two paratopes. The value of n_1 is assumed to be similar to that obtained for the same interaction on the surface, therefore we used n_1 = 7. We computed the equilibrium condition of the bimolecular reaction considering the total concentrations of binding sites in solution for Ab1 and Ab2, which are given by n_2c_2 and n_1c_1, respectively. Accordingly, the concentration c_2* of free Ab2 antibody available for the binding with Ab1 on the surface is given by:

$$c_2^* = \frac{(n_2c_2 - n_1c_1) - K_d + \sqrt{(n_1c_1 - n_2c_2 + K_d)^2 + 4K_dn_2c_2}}{2n_2} \quad \text{(S4)}$$

The value of K_d =1.3 nM is chosen so that the measured initial slope of the Ab2 binding curves $\sigma(t)$ show a linear dependence as a function of c_2*. Analogously, the concentration c_1* of available Ab1 in solution is also affected by the binding with Ab2 and is obtained as

$$c_1^* = c_1 - \frac{n_2}{n_1}(c_2 - c_2^*) \quad \text{(S5)}$$

S4 Modelling of the 3-stage assay's interactions

The amount of molecules binding on the assay spots was simulated by numerically solving a system of 3 coupled differential equations and using the parameters from Table 2 (specifically, for RNA/DNA binding simulation, we considered kinetic parameters of miRNA21). Each equation describes binding of specific injected target, i.e. the formation of RNA/DNA hybrids, Ab1 binding on formed hybrids and the formation of Ab1/Ab2 pairs on surface:

$$\frac{d\phi_0}{dt} = k_{on,0}c_0(1 - \phi_0(t)) - k_{off,0}\phi_0(t) \quad \text{(S6)}$$

$$\frac{d\phi_1}{dt} = k_{on,1}c_1^*(\phi_0(t) - \phi_1(t)) - k_{off,1}\phi_1(t) \quad \text{(S7)}$$

$$\frac{d\phi_2}{dt} = k_{on,2}c_2^*(\phi_1(t) - \phi_2(t)) - k_{off,2}\phi_2(t) \quad \text{(S8)}$$

where indices 0,1,2 correspond to RNA-DNA (hybrid) binding, Ab1-hybrid binding, Ab2-Ab1 binding, respectively. ϕ_i corresponds to the fraction of occupied surface binding sites of the interaction i, $k_{on,i}$ and $k_{off,i}$ are the association and dissociation rate, respectively, and c_i denotes the injected concentration of the corresponding analyte. Specifically, unlike

RNA/DNA and Ab1-hybrid interactions, where binding occurs in stoichiometric ratio of 1, a single Ab1 contains n_1 binding sites for Ab2, therefore, the surface amount of Ab2 is obtained as ϕ_2 times n_1. Equations S6-S8 neglect steric effects limiting the surface density of antibodies on the sensor surface and thus are valid for small values of ϕ_0, corresponding to small concentrations of miRNA in solution. Furthermore, considering the Ab1-Ab2 binding in solution, presence of Ab2 in the cuvette inevitably effects the binding of Ab1, and vice versa, therefore, Equations S7 and S8, which describe binding of Ab1 and Ab2, respectively, should be modified to account for the decrease in concentration of each analyte due to their interaction in solution according to Equations S4 and S5. Corrected concentrations of both Ab1 and Ab2 are marked c_1^* and c_2^*, respectively. To convert from fractional surface coverage to mass surface density, solutions were further multiplied by the asymptotic values of surface density Σ_∞, where $\Sigma_{\infty,0}$ was observed experimentally, and $\Sigma_{\infty,1}$ and $\Sigma_{\infty,2}$ were calculated considering mass and stoichiometric ratios. Given that a single hybrid binds a single Ab1, the maximum mass surface density of Ab1 that can bind to the hybrid is related to the bound miRNA via their mass ratio, i.e.: $\Sigma_{\infty,1}/\Sigma_{\infty,0} = m_{Ab}/m_0$. In contrast, Ab1 and Ab2 have roughly the same mass but about 7 Ab2 can bind a single Ab1, therefore the maximum Ab2 mass density is given by $\Sigma_{\infty,2} = n_1\Sigma_{\infty,1}$. Numerical solutions are shown in Figure S1. The system was solved considering 5 pM concentration of miRNA, 2.5 nM of Ab1 and 25 nM of Ab2. All incubation times are 30 min.

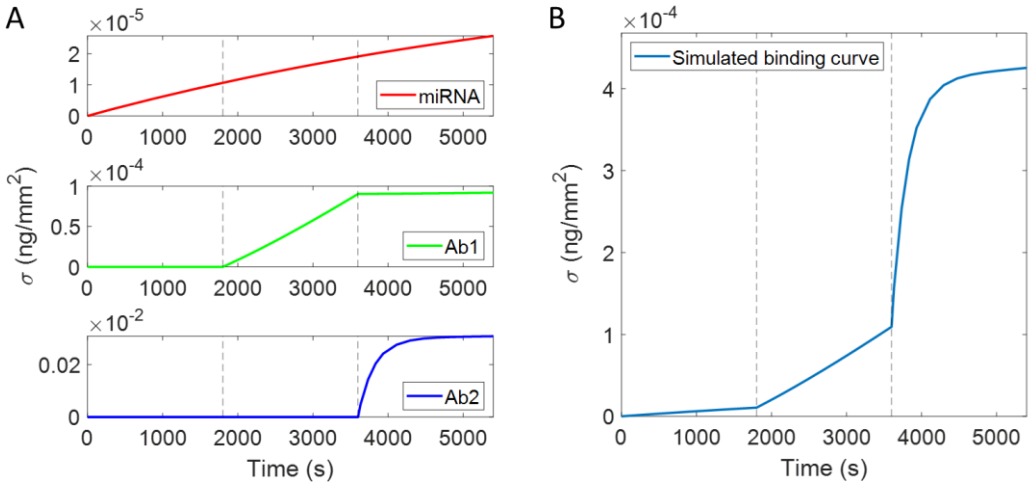

Figure S1. Simulation of assay response. **A)** Simulated binding for all three injections during the course of the experiment. Each injection is indicated by the vertical dashed line, each 30 min apart, followed by an increase of mass of injected analyte. miRNA binding is shown in red, during the course of the experiment miRNA binding is not reaching the equilibrium, as expected considering the low concentration. Ab1 binding is shown in green. Decrease of effective Ab1 concentration following the injection of Ab2 results in strongly reduced binding of Ab1. Binding of Ab2 is shown as dark blue. **B)** Complete binding curve, simulated with Equations S6, S7, S8, obtained by summing the numerical solutions to these equations at specific time. Vertical lines represent the injection points of each analyte. Total bound mass is shown on the y-axis.

Same simulation was carried out considering larger Ab2 concentration of 67.5 nM (Figure S2). Results suggest that the decrease in adsorbed mass in Figure 4a (brown) is a result of detachment of Ab1 and Ab2 from the surface, following the change in equilibrium due to a decrease of c_1^* in solution upon addition of Ab2 (Equations S5).

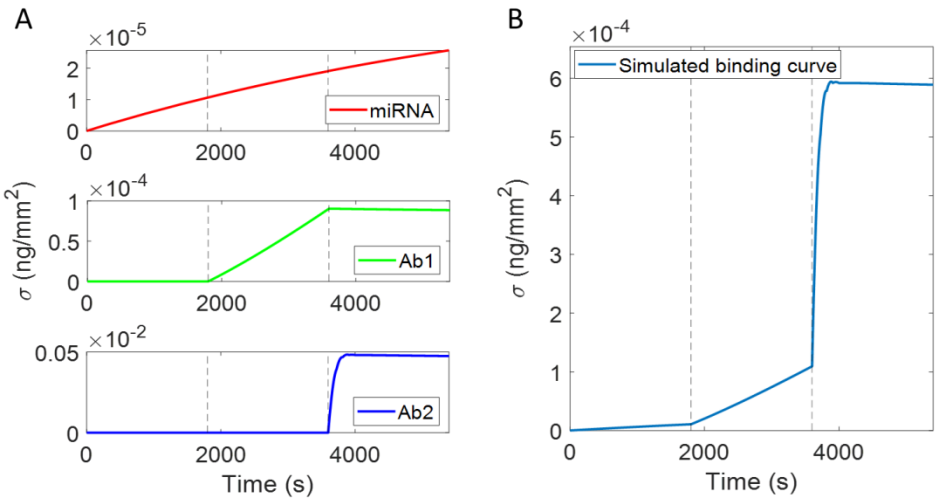

Figure S2. Simulation of assay response at large concentration of Ab2. **A)** Simulated binding for all three injections (concentration of Ab2 is 67.5 nM) during the course of the experiment. **B)** Complete binding curve. The decrease in signal after the final injection is associated with the decrease of Ab1 surface density on the sensor surface (Figure S2 A green) and detachment of Ab2 (Figure S2 A blue).

Figure S3 shows the decrease effect in greater detail. Binding curves for all three analytes during the final injection is shown in panel A. Specifically, binding plot of Ab2 (dark blue) is zoomed in to emphasize the decrease. The decrease of mass of Ab1 represents the detaching of Ab1 and is an effect of change in effective Ab1 concentration due to the Ab1-Ab2 formation in solution. The kinetics of this detachment is much slower than the binding kinetics of Ab2 on the surface. This results in the formation of a local maximum, roughly 10 minutes after the injection, after which the mass of bound Ab2 starts to decrease. This is all observed in Figure S3B, as an enlarged view of the local maximum. Extending the incubation time for Ab2 even further (and hence the time of the experiment), it is possible to obtain the equilibrium of the system which onsets well after the asymptotic equilibrium of miRNA on the surface. It's worth noting that the calculated mass density at the equilibrium can be slightly larger than the observed peak, therefore the peak presents a local maximum.

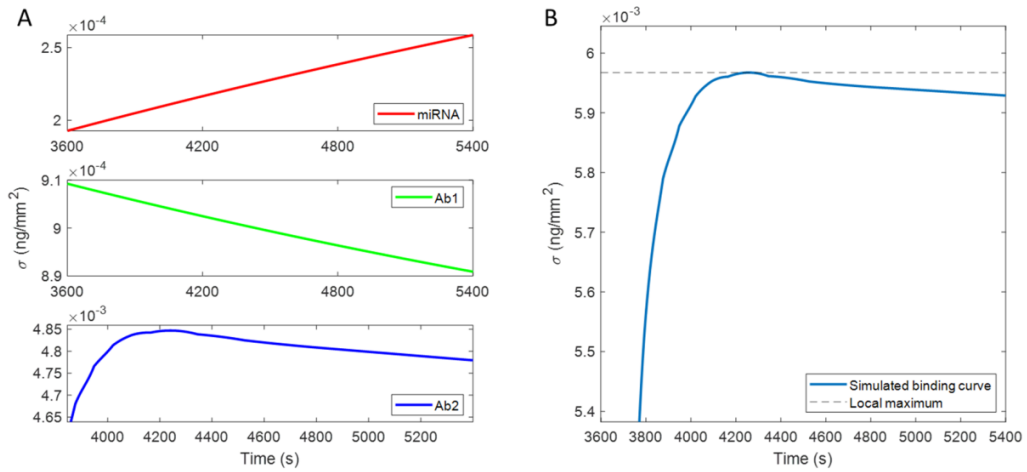

Figure S3. Simulation of the non-monotonic response after addition of Ab2. **A)** Simulated binding for all three injections during 2h incubation time of Ab2 (concentration of Ab2 is 67.5 nM). Plot showing the binding of Ab2 is zoomed in to emphasize the decrease. **B)** Complete binding curve during the same time, zoomed in to emphasize the decrease. Dashed line represents the maximum value obtained before the decrease. Continuation of this simulation leads to another increase of total bound mass, preceded by miRNA reaching equilibrium, which ends in a global maximum at highly greater value than the observed peak.

S5 Calculation of the amplification factor

The behavior of the amplification factor reported in Figure 5 was calculated as the ratio of total adsorbed mass (miRNA, Ab1 and Ab2) after 1.5h and the simulated miRNA mass that would be bound after the same amount of time and without the presence of both Ab1 and Ab2, i.e.:

$$Amplification\ factor = \frac{\Sigma_{\infty,0}\phi_0(t_0+t_1+t_2)+\Sigma_{\infty,1}\phi_1(t_1+t_2)+\Sigma_{\infty,2}\phi_2(t_2)}{\Sigma_{\infty,0}\phi_0(t_0+t_1+t_2)} \quad \text{(S9)}$$

where t_0 represents the incubation time of miRNA, t_1 and t_2 are incubation times of Ab1 and Ab2, respectively. The values of Σ_∞ are given by the number surface density of each analyte times its molecular mass. Considering that, for small miRNA concentrations, the maximum number surface density of Ab1 corresponds to the number surface density of DNA-RNA hybrids and that the maximum number surface density of Ab2 corresponds to the number surface density of Ab1 times the number of sites n_1 per Ab1 molecules, Equation S9 can be further simplified as:

$$Amplification\ factor = 1+\frac{m_{Ab}}{m_0}\frac{\phi_1(t_1+t_2)+n_1\phi_2(t_2)}{\phi_0(t_0+t_1+t_2)} \quad \text{(S10)}$$

where m_0 and m_{Ab} are the molecular mass of miRNA and of IgG antibodies, respectively. Accordingly, the maximum amplification factor is obtained when both ϕ_1 and ϕ_2 equal ϕ_0, thus yielding to $1+m_{Ab}(1+n_1)/m_0$.

S6 Quantification of background signal due to non-specific binding

The selected miRNA strands displayed a negligible cross-interaction with non-complementary DNA probes on the surface. This is shown in Figure 2a, in which all five miRNAs considered are added one by one in the same measuring cartridge. The signal measured form each DNA spot increases only when the complementary miRNA is added. The binding in the regions outside the spots is also negligible (black line).

As shown in Figure 1b, the non-specific binding of Ab1 and Ab2 remains undetectable on the sensor surface outside the DNA-spotted regions (black line), whereas it is very small but measurable on spots of single strand DNA not hybridized with RNA (red line). We characterized the level of background RPI signal due non-specific binding of Ab2 in order to estimate the LOD of detection for miRNAs. A typical value of such non-specific background due to Ab2 binding is represented by the red line in Figure 1b, which shows an average surface density of Ab2 on single strand DNA spots of 6 pg/mm^2 and a standard deviation of 1.6 pg/mm^2. Accordingly, a signal was considered specific if larger than 3σ from such background, corresponding to a threshold of about 11 pg/mm^2.

As additional control experiment, we measured the surface density due to Ab2 binding in absence of Ab1 in the optimal conditions selected for the assay, consisting in the concentrations and times used to obtain the results reported in Figure 6. We added in the measuring cartridge all the five miRNAs and then Ab2 at the working concentration of 25 nM. The measured surface density is reported Figure S4. These results confirm that the sole contribution of non-specific binding of Ab2 on top of the DNA/RNA hybrid at the end of the total measuring time of 1.5 h results in a surface density increment of about 4 pg/mm^2, hence slightly smaller than the estimate of the total background level described above. The subsequent addition of Ab1 at 4.5 nM induced a rapid increase of the RPI signal, followed by a decrease, similarly to the behaviour reported in Figure 4a, in which the addition of the antibodies followed the standard sequence Ab1 then Ab2. However, in the experiment reported in Figure S4, the non-specific binding on control spots, previously exposed to Ab2, is larger, and the maximum amplitude reached on the specific spots is smaller because the binding of Ab1 to the DNA/RNA hybrid on the surface is partially hindered by the binding with Ab2 in solution.

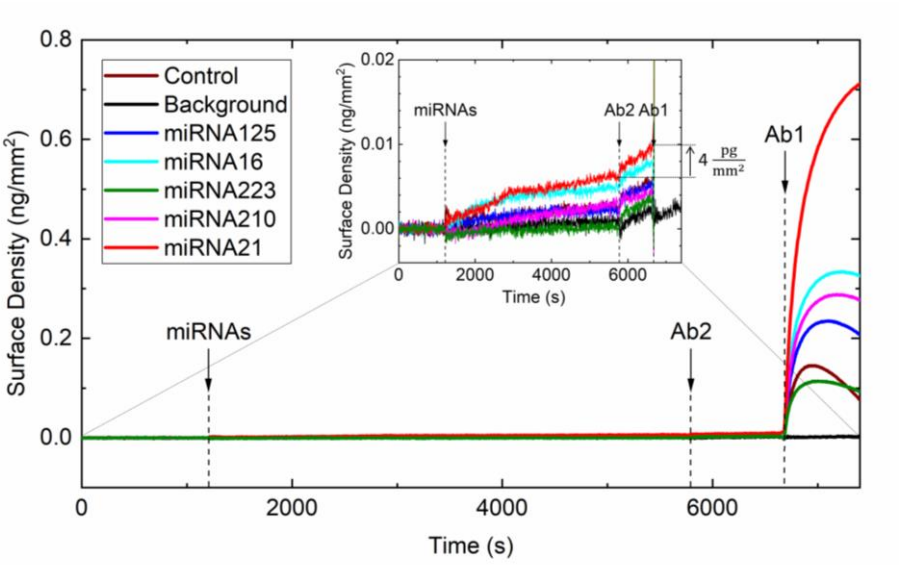

Figure S4. Non-specific binding of Ab2. Surface density measured by RPI upon sequential addition of miRNAs, Ab2 and Ab1 at the times indicated by the vertical lines. The concentrations of miRNAs in the measuring cartridge were 15 pM, 27.9 pM, 27 pM, 88 pM and 209.7 pM for miRNA125, miRNA16, miRNA223, miRNA210 and miRNA21, respectively. The concentration of Ab2 and Ab1 were 25 nM and 4.5 nM, respectively. Colors correspond to different DNA probe spots, targeting the miRNAs indicated in the Figure legend. The black points represent the background signal measured outside the spots area. Inset: enlarged view of the plot before the addition of Ab1.

References

Giavazzi, F., Salina, M., Ceccarello, E., Ilacqua, A., Damin, F., Sola, L., Chiari, M., Chini, B., Cerbino, R., Bellini, T., Buscaglia, M., 2014. A fast and simple label-free immunoassay based on a smartphone. Biosens. Bioelectron. 58, 395–402. https://doi.org/10.1016/j.bios.2014.02.077

Giavazzi, F., Salina, M., Cerbino, R., Bassi, M., Prosperi, D., Ceccarello, E., Damin, F., Sola, L., Rusnati, M., Chiari, M., Chini, B., Bellini, T., Buscaglia, M., 2013. Multispot, label-free biodetection at a phantom plastic–water interface. Proc. Natl. Acad. Sci. 110, 9350–9355. https://doi.org/10.1073/pnas.1214589110

Nava, G., Ceccarello, E., Giavazzi, F., Salina, M., Damin, F., Chiari, M., Buscaglia, M., Bellini, T., Zanchetta, G., 2016. Label-free detection of DNA single-base mismatches using a simple reflectance-based optical technique. Phys. Chem. Chem. Phys. 18, 13395–13402. https://doi.org/10.1039/C5CP08017G

SantaLucia, J., 1998. A unified view of polymer, dumbbell, and oligonucleotide DNA nearest-neighbor thermodynamics. Proc. Natl. Acad. Sci. 95, 1460–1465. https://doi.org/10.1073/pnas.95.4.1460

Weber, G., 2015. Optimization method for obtaining nearest-neighbour DNA entropies and enthalpies directly from melting temperatures. Bioinformatics 31, 871–877. https://doi.org/10.1093/bioinformatics/btu751

Zadeh, J.N., Steenberg, C.D., Bois, J.S., Wolfe, B.R., Pierce, M.B., Khan, A.R., Dirks, R.M., Pierce, N.A., 2011. NUPACK: Analysis and design of nucleic acid systems. J. Comput. Chem. 32, 170–173. https://doi.org/10.1002/jcc.21596